Brazilian Journal
of Chemical
Engineering

ISSN 0104-6632
Printed in Brazil
www.abeq.org.br/bjche

Vol. 23, No. 04, pp. 473 - 486, October - December, 2006

NUMERICAL SIMULATION AND EXPERIMENTAL STUDY OF NON-NEWTONIAN MIXING FLOW WITH A FREE SURFACE

M. Dular[1*], T. Bajcar[1], L. Slemenik-Perše[2], M. Žumer[1] and B. Širok[1]

[1]University of Ljubljana, Faculty of Mechanical Engineering,
Phone: + 386 (0)1 4771-453; Fax : + 386 (0)1 2518 567,
Aškerčeva 6, SI-1000 Ljubljana, Slovenia
E-mail: matevz.dular@fs.uni-lj.si,
E-mail: tom.bajcar@fs.uni-lj.si, E-mail: miha.zumer@uni-lj.si,
E-mail: E-mail: brane.sirok@fs.uni-lj.si
[2]University of Ljubljana, Faculty of Chemistry and Chemical Technology, Aškerčeva 5,
SI-1000 Ljubljana, Slovenia / Institute of Chemistry, Hajdrihova 19,
SI-1001 Ljubljana, Slovenia
E-mail: lidija.slemenik.perse@ki.si

(Received: October 4, 2005 ; Accepted: May 31, 2006)

Abstract - The object of this work was to evaluate the capability of numerical simulation to predict different features of non-Newtonian fluid mixing process. A relatively simple impeller (six bladed vane rotor) was used for the mixing of carboxymethyl cellulose. A LDA method was used to measure the tangential velocity at two points inside the mixing vessel. Using visualization, a significant vortex above the impeller was observed. The shape of the free surface was determined by a geometrical reconstruction of the images of the illuminated section. Torque on the impeller shaft was measured to determine the characteristics of the fluid.
Fluent program package was used for the simulation. The problem is challenging since the effects of non-Newtonian fluid, mixing process and free surface have to be included in the simulation. The comparison between the experimental and numerical results confirms the accuracy of the simulations.
Keywords: Non-Newtonian fluids; Mixing; LDA, Visualization; CFD; Free surface.

INTRODUCTION

The use of highly viscous non-Newtonian fluids is very frequent in many industrial operations, particularly in mixing processes. Such fluids often have complex rheological properties, which can increase operating costs and can create other problems during the mixing process.

The viscosity, as one of the most important property of the fluid, has a great significance in processes, in which the rheological properties of the fluid are changing with time. Due to a close relation of the viscosity to torque on the impeller in the mixing vessel, the changing of the viscosity reflects in torque changes. If the viscosity increases too much, torque increases over the limit, which can lead to destruction of the motor. To eliminate such problems, the viscosity should be monitored continuously over the whole process. Usually the viscosity is measured in rheometer by rheological tests. For the case of fermentation broths and other non-homogeneous fluids rheological measurements in rheometers are not always accurate, due to gravity settling of the suspended particles and/or other forms of phase separation in suspensions. For these fluids, another method of viscosity measurements should be

*To whom correspondence should be addressed

therefore applied. One of the ideas is to measure viscosity during mixing indirectly by measuring the torque on the impeller as a function of impeller rotational frequency (Slemenik and Žumer, 2004).

For simple pseudoplastic fluids the viscosity can be described by the power law:

$$\eta = k \ \dot{\gamma}^{\,n-1} \tag{1}$$

where k and n are consistency index and flow behaviour index, respectively. For such fluids the viscosity in mixing vessel can be determined by using the relation, proposed by Metzner and Otto (1957):

$$\dot{\gamma} = K_s N \tag{2}$$

where the constant K_s is reported to be dependent on the geometry of the system only (Harnby et al., 1992, Ekato, 1991 and Fryer et al., 1997), but lately some authors (Brito et al., 1998, Slemenik and Žumer, 2004) report also on dependence of K_s on fluid properties. For mixing the 2 % CMC solution with the present impeller a value of 16 was used for the K_s (Slemenik-Perše, 2004).

Combining equations (1) and (2), one can obtain the viscosity as a function of impeller rotating frequency:

$$\eta = k \ \left(K_s N\right)^{n-1} \tag{3}$$

The non-Newtonian mixing Reynolds number is then defined as:

$$\mathrm{Re} = \frac{\rho N D^2}{\eta} = \frac{\rho D^2}{k K_s^{n-1} N^{n-2}} \tag{4}$$

In order to get exact results of shear dependent viscosity of non-Newtonian fluids, indirectly during mixing, by measuring the torque and impeller rotating frequency, shear field around impeller in mixing vessel should be precisely defined. In the present work the shear field around six-bladed vane impeller was determined by Laser Doppler anemometry (LDA). The LDA method is very frequently used for measurements of laminar and turbulent velocities in transparent fluids. It has an important advantage since the probe lies outside the mixing vessel and does not interfere with the flow pattern (Mavros, 2001). A laser beam is split in two coherent beams, which cross at a desired point inside the mixing vessel. Small particle that crosses the intersection volume scatters light, which is captured by a photo detector. The velocity of the particle crossing the intersection volume is determined from the analysis of the change in the intensity fluctuations on the photo detector (Mavros, 2001).

Very complex simulations of non-Newtonian fluid flow are still rare. The present problem includes non-Newtonian flow, mixing process and the presence of a free surface. Many papers deal only with a part of the present paper - for example Shao and Lo (2003) deal with a 2-dimensional non-Newtonian free surface “dam break” simulation, Boyer et al. (2004) developed their own numerical method and tested it on different non-Newtonian flow problems (channel under shear, filling of a tank, break-up of a jet). Kelly and Gigas (2003) used CFD for simulations of non-Newtonian fluid mixing, but did not deal with a free surface problem.

The paper reports on experimental velocity measurements for a highly viscous non-Newtonian fluid in a mixing vessel with a six-bladed vane impeller. Laser-Doppler anemometry was used for measurements of tangential velocity component at two positions inside the mixing vessel.

To observe the characteristic vortex above the impeller a tracer fluid was injected into the mixing vessel. A vortex between the impeller and free surface was observed and recorded using a CCD camera.

A reflection of a laser light sheet from the free surface of the fluid in the vessel was captured with a CCD camera. The shape of the free surface was later reconstructed from the images.

Torque on the shaft of the impeller at different rotational frequencies was measured.

The rheological properties of CMC solution were determined by a rotational controlled stress rheometer.

Although a steady flow was observed during the experiments, an unsteady numerical simulations at three different rotational frequencies of the mixing process had to be performed because of the use of limitations of the volume of fluid (VOF) model. Fluent 6.1.18 software was used. A sliding mesh approach was used to include the rotation of the rotor. A VOF multiphase model had to be used since a free surface between the carboxymethyl cellulose solution and air existed. To describe the dependence of the fluid viscosity to the shear rate a power law (Eqn. 1) was used.

Comparisons between experimental results and predictions of simulations of velocities, vortex shapes, free surface shapes and torques on the shaft show very good correlations.

Results promise a good possibility of predicting flow characteristics and optimisation of complex industrial mixing processes in the future.

EXPERIMENTAL SET-UP

Carboxymethyl cellulose - CMC (Blanose Cellulose Gum 7HF, from Hercules, Aqualon) was used as highly viscous non-Newtonian fluid. For the experiments, a concentration of 2 % wt. of CMC was prepared by dissolving dry powdered CMC in distilled water at ambient temperature.

The rheological properties of CMC solutions were determined by a rotational controlled stress rheometer (HAAKE RheoStress RS150), equipped with a cone-and-plate sensor system (C 60/4°). The rheological characterization was performed under steady shear conditions (flow curves). The flow curves (η vs. $\dot{\gamma}$) were examined in the shear rate range $1<\dot{\gamma}<100\ s^{-1}$, which was determined regarding to the shear rate range established around impeller during the mixing process (Fig.1). The viscosity could be determined with an uncertainty level of ± 3 % of the measured value.

The viscosity of the solution was in the range from 1 to 10 Pa s. The behaviour of the solution can be described by the power law (Eqn. 1). Constants k = 14.96 and n = 0.4208 were determined.

All experiments were conducted in a flat-bottomed plexiglass vessel with inside diameter D_T = 190 mm and the height of the fluid inside the vessel H = 220 mm. The vessel was equipped with six-bladed vane with a diameter D = 160 mm and height h = 150 mm. The distance between the vessel bottom and blades was Z = 35 mm (Fig. 2). All experiments were performed at ambient temperature (22°C to 25°C).

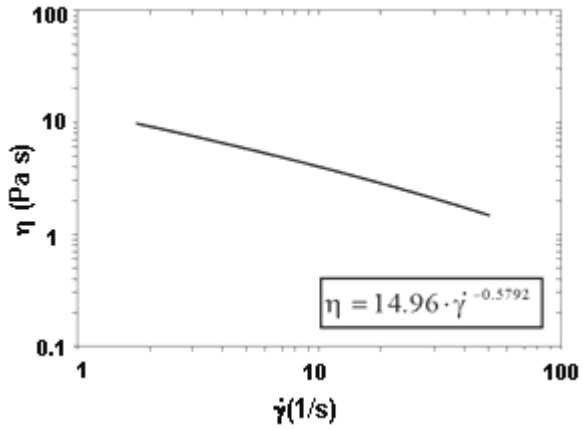

Figure 1: The flow curves (viscosity vs. shear rate) for 2% CMC solution at 25°C.

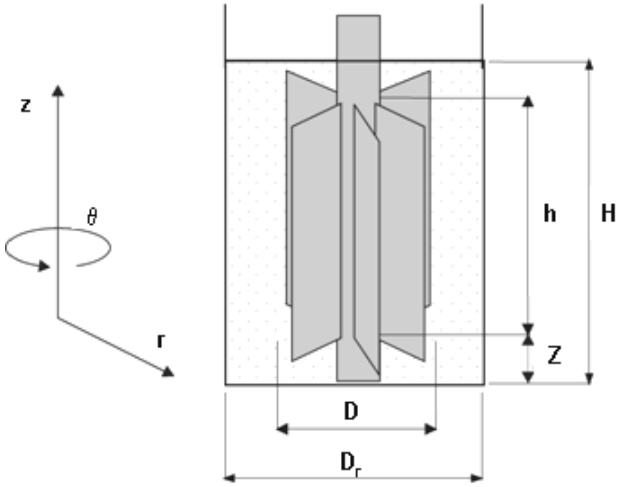

Figure 2: Six-bladed impeller inside the vessel with noted dimensions and coordinate system.

LDA Measurements

The velocity measurements were performed by using two-component laser-Doppler anemometer (LDA) from TSI with argon-ion laser Spectra Physics model 2016. The measurement volume of LDA system was directed at a desired position in the vessel by optical probe TSI model 9275-1, which was mounted on the three-axis traverse system (Fig. 3). The measurements were performed at three different impeller rotating frequencies (30, 60 and 90 rpm) in the r-z plane (Fig. 2) with presumed axis-symmetric flow and velocity field, respectively. The rotational frequency of the impeller was measured with an incremental encoder - the uncertainty of the measurement was in the order of 2 % of the measured value.

The mixing flow was always in the laminar regime – the Reynolds number (Eqn. 4) was equal to Re = 2.85, 8.52 and 16.17, for 30, 60 and 90 rpm, respectively.

Two measurement points were chosen in the measurement plane. At a distance r = 90 mm from the centre of the impeller shaft (r = 0) on planes z = 135 mm and z = 196 mm from the bottom of the vessel. Only the tangential velocity component (in direction of the impeller rotation) was measured in detail. Measurements of axial and radial velocity components revealed that these are of insignificant magnitude (while the tangential velocity component exceeds 0.5 m/s, the axial and radial velocities lie in the order of 0.01 m/s and 0.05 m/s, respectively (case of rotating frequency of 60 rpm)) and that their evolution in time is not that interesting for the present problem. Typical data rate of the LDA system was in the range of 10 kHz.

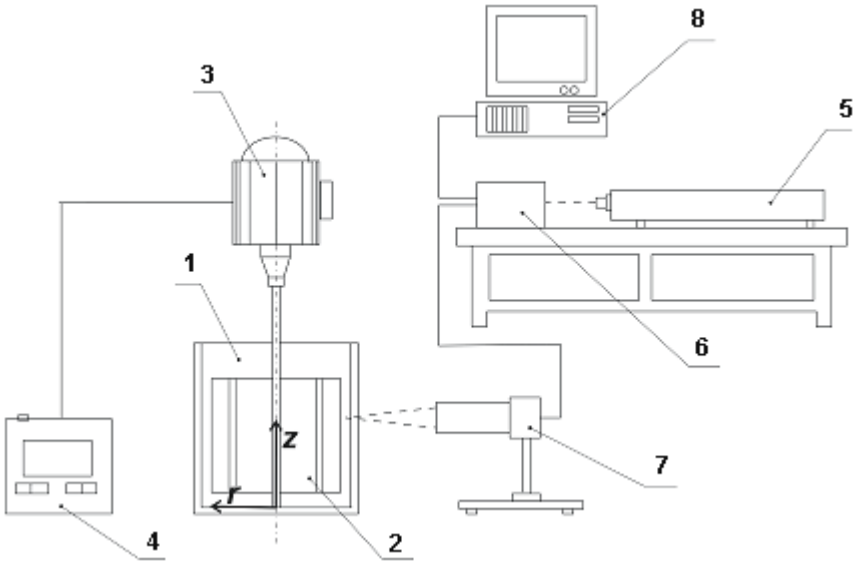

1) mixing vessel;
2) impeller;
3) electric motor;
4) voltage regulator;
5) laser light source
6) optical and electronic LDA equipment;
7) laser probe on a traverse system;
8) PC for analysis and display of results.

Figure 3: Experimental set-up for the velocity measurements in the mixing vessel with LDA system:

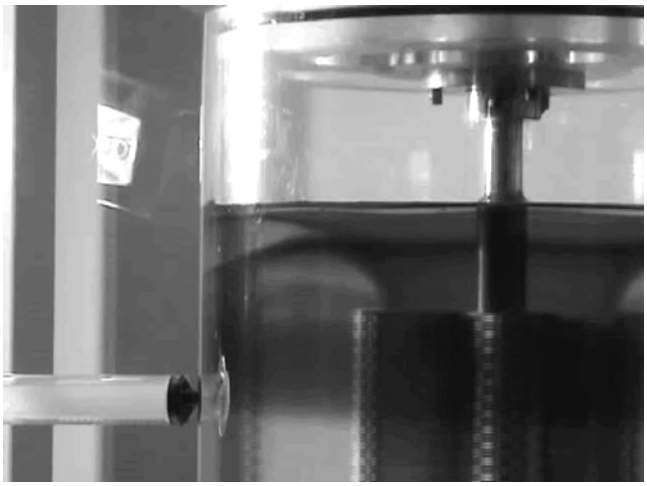

Figure 4: Injection of the tracer fluid into the vessel and formation of the vortex above the impeller.

Visualization of the Vortex

To determine the flow pattern a tracer fluid (CMC with added $KMnO_4$) vas slowly injected into the vessel at level z = 150 mm – Fig. 4.

It took between 15 and 35 s for the vortex to become visible (depending on rotational frequency). The vortex forms as a result of pressure gradients – the fluid rotates the fastest near the impeller and the slowest near the free surface (and near the vessel walls), which results in lower pressure region near the free surface and higher pressure deeper in the vessel. The fluid is forced from the top of the impeller upwards near the vessel wall towards the free surface, then toward the shaft of the impeller, down, toward the vessel wall and again up toward the free surface. The pressure difference is small – the maximal z-velocity is about 9 mm/s for the case of rotational frequency 60 rpm.

The mean boundary of the vortex for each of the rotational frequencies was determined using the maximal gradient finding technique (Širok et al., 2002). The position of maximal gradient of gray level in the image defines the section boundary (the recorded images were transformed into 8 bit resolution – 256 levels of gray level).

The intensity of the gray level transition can be defined as a two component gradient ∇A(i,j):

$$\nabla A(i,j) = \begin{bmatrix} \nabla A_i(i,j) \\ \nabla A_j(i,j) \end{bmatrix} = \begin{bmatrix} \dfrac{\partial A(i,j)}{\partial i} \\ \dfrac{\partial A(i,j)}{\partial j} \end{bmatrix} \tag{5}$$

where the scalar value (=norm) of Eqn. 5 is:

$$\left\| \nabla A(i,j) \right\| = \sqrt{\left(\frac{\partial A(i,j)}{\partial i} \right)^2 + \left(\frac{\partial A(i,j)}{\partial j} \right)^2} \tag{6}$$

The position of the vortex boundary is then determined by the position of the pixel in each column i where the maximum value of gradient appears:

$$(i_m, j_m) = \max \left[\sqrt{\left(\frac{\partial A(i,j)}{\partial i} \right)^2 + \left(\frac{\partial A(i,j)}{\partial j} \right)^2} \right]_{i=konst} \tag{7}$$

$$i = 1,\ 2,\ \ldots, n$$

i_m and j_m represent the coordinates.

The results of experimental visualization can be seen together with prediction of numerical simulation in Fig. 11.

Free Surface Shape Determination

A vertical laser light sheet was used to "cut" a section of the free surface. The images of the illuminated section were recorded by a CCD camera that was positioned at a determined distance and angle to the vertical direction (Fig. 5).

The coordinates of the section on the free surface were determined by the already described edge finding algorithm. The actual position of the surface was then reconstructed using simple geometrical transformations. The results of the free surface shape measurements are presented together with the predictions of numerical simulations in Fig. 12.

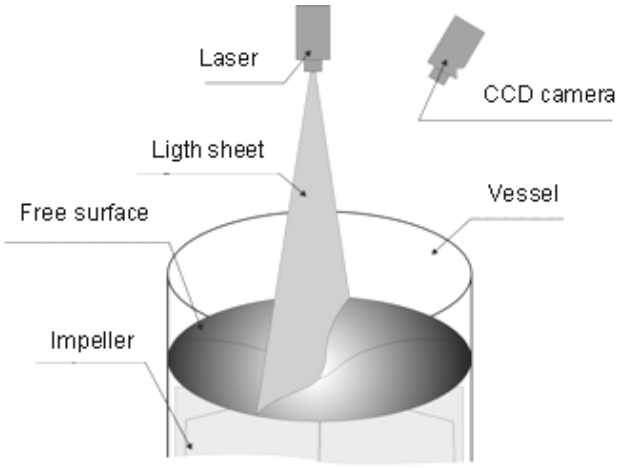

Figure 5: Determining of the shape of the free surface.

Shaft Torque Measurements

The torque on the impeller shaft was measured with the HBM T20WN/2NM sensor. The measurements were then averaged during a period of 10 minutes for each impeller rotating frequency. The declared accuracy of the sensor is ± 0.2 %. The uncertainty of the measurements was estimated to less than ±1 %.

The results of experimental measurements are shown together with predictions of numerical simulations in Fig.13.

NUMERICAL SIMULATION

Although a steady flow was observed during experiments unsteady numerical simulations at three different rotational frequencies of the mixing process had to be performed because of the use of VOF model with geometric reconstruction scheme, which does not allow a steady computation.

Multiphase Free Surface Model

The VOF formulation (Hirt and Nichols, 1981) relies on the fact that two or more fluids (or phases) are not interpenetrating. For each additional phase that is added to the problem, a new variable is introduced: the volume fraction of the phase in the computational cell. In each control volume the volume fractions of all phases sum to unity. The fields for all variables and properties are shared by the phases and represent volume-averaged values, as long as the volume fraction of each of the phases is known at each location. Thus the variables and properties in any given cell are either purely representative of one of the phases, or representative of a mixture of the phases, depending upon the volume fraction values. In other words, if the q-th fluid's volume fraction in the cell is denoted as α_q, then the following three conditions are possible:

- $\alpha_q = 0$: the cell is empty of the q-th fluid.
- $\alpha_q = 1$: the cell is full of the q-th fluid
- $0<\alpha_q<1$: the cell contains the interface between the q-th fluid and one or more other fluids.

Based on the local value of α_q, the appropriate properties and variables are assigned to each control volume within the domain. The tracking of the interface(s) between the phases is accomplished by the solution of the continuity equation for the volume fraction of one (or more) of the phases. For the q-th phase, this equation has the following form:

$$\frac{\partial \alpha_q}{\partial t} + \vec{v}_m \cdot \nabla \alpha_q = 0 \tag{8}$$

The volume fraction equation is not solved for the primary phase for which the volume fraction is computed on the base of the following constraint:

$$\sum_{q=1}^{n} \alpha_q = 1 \tag{9}$$

The properties appearing in the transport equations are determined by the presence of the component phases in each control volume. In a two-phase system (the phases are represented by the subscripts 1 and 2), and the volume fraction of the second phase is being tracked, the density in each cell is given by:

$$\rho_m = \alpha_2 \rho_2 + (1-\alpha_2)\rho_1 \tag{10}$$

and similarly the viscosity:

$$\nu_m = \alpha_2 \nu_2 + (1-\alpha_2)\nu_1 \tag{11}$$

A single momentum equation is solved throughout the domain, and the resulting velocity field is shared among the phases. The momentum equation, shown below, is dependent on the volume fractions of all phases through the properties ρ_m and η_m.

$$\begin{aligned} &\frac{\partial}{\partial t}\left(\rho_m \vec{v}_m\right) + \nabla \cdot \left(\rho_m \vec{v}_m \vec{v}_m\right) = \\ &= -\nabla p + \nabla \cdot \left[\eta_m \left(\nabla \vec{v}_m + \nabla \vec{v}_m^{T}\right)\right] + \rho_m \vec{g} + \vec{F} \end{aligned} \tag{12}$$

One limitation of the shared-fields approximation is that in cases where large velocity differences exist between the phases, the accuracy of the velocities computed near the interface can be adversely affected.

A second order upwind interpolation scheme was used to obtain the face fluxes whenever a cell is completely filled with one phase or another. The geometric reconstruction scheme was used when the cell is near the interface between two phases.

The geometric reconstruction scheme represents the interface between fluids using a piecewise-linear approach. It assumes that the interface between two

fluids has a linear slope within each cell, and uses this linear shape for calculation of the advection of fluid through the cell faces.

The first step in this reconstruction scheme is calculating the position of the linear interface relative to the centre of each partially filled cell, based on information about the volume fraction and its derivatives in the cell. The second step is calculating the advecting amount of fluid through each face using the computed linear interface representation and information about the normal and tangential velocity distribution on the face. The third step is calculating the volume fraction in each cell using the balance of fluxes calculated during the previous step.

Non-Newtonian Model

A power law model (Eqn. 1) was used for modelling the non-Newtonian fluid properties. The values for the constants that were used in the simulation were the same as those found at the experiment (k = 14.96 and n = 0.4208) (Fig.1).

SIMULATION

A structured mesh was used for the meshing of the domain (Fig. 6). To reduce the computational effort, only 1/6 (one blade passage) of the domain was modelled and periodic conditions were applied to the boundaries.

To check the influence of spatial and time discretization, a study of these parameters was made. Results are presented in Tab. 1.

Three mesh sizes were tested. In all cases a converged solution was achieved and very little influence of the mesh size was observed. Based on a comparison of the mean tangential velocity component in a point (r = 90, z = 135), a discretization error of 0.4 % was estimated. Finally a mesh with approximately 225000 nodes was used for simulations. The mesh was refined near the walls of the impeller, near the vessel wall and at the interface between the rotating and steady part of the mesh (Fig. 6).

Time step size of 10^{-3} s (1000 time steps per revolution for the case of rotational frequency N = 60 rpm) was used for the simulations. When a shorter time step ($0.5*10^{-3}$s) was used, a slightly higher velocity was predicted.

The convergence criterion was determined by observing the evolution of velocity magnitude in a certain point inside the domain (r = 90, z = 135). The monitored flow parameters were always converged after the sum of the imbalance of the transport equations between iterations over all cells in the computational domain (residuals of the variables: pressure, velocity and volume fraction) fell below $5*10^{-3}$ (after the error residuals drop by 2.5 orders of magnitude).

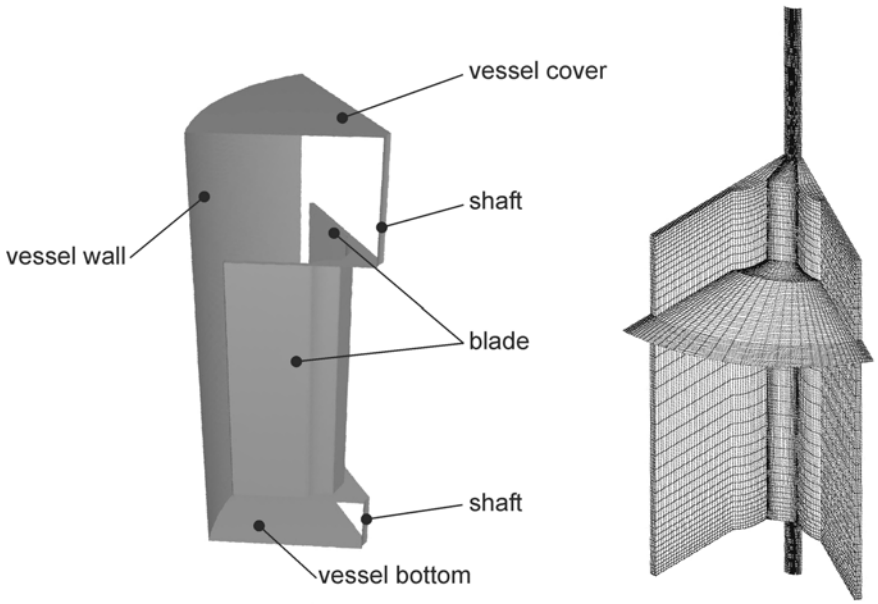

Figure 6: Computational domain and mesh.

Table 1: Spatial and temporal discretization study for rotational frequency N = 60 rpm in point r = 90, z = 135.

Grid size	Time step (10^{-3} s)	Mean velocity (m/s)
~ 100000	1	0.0798
~ 225000	1	0.0821
~ 800000	1	0.0852
~ 225000	0.5	0.0834

Eventually a value of $5*10^{-4}$ was used as the criterion for a converged time step. Approximately 20 iterations per time step were needed to obtain a converged solution. The iteration error of 0.05 % was estimated.

Conditions applied for the simulations were the following:

- Flow: Since the mixing flow was always in the laminar regime (the Reynolds number (Eqn. 4) was equal to Re = 2.85, 8.52 and 16.17, for 30, 60 and 90 rpm, respectively), no turbulence model was applied. The highest numerically predicted velocity in the vessel was in the range of 0.5 m/s (case of rotating frequency N = 60 rpm), which confirms our hypothesis of laminar flow regime.
- Boundary conditions: No slip wall condition was applied to vessel wall, bottom and to the shaft and the blades of the impeller (the near wall treatment problem was eliminated by the assumption of laminar flow). A pressure outlet boundary condition with atmospheric pressure 1 bar was assigned to vessel cover.
- A time step 10^{-3} s was used for all simulations but one where the temporal discretization was put into question (Tab. 1).
- Similar to the experiment CMC fluid properties were patched into the domain from the bottom of the vessel up to the level z = 220mm as an initial condition. Above this level (z = 220mm) air properties were considered.
- Rotational frequency of N = 30, 60 and 90 rpm (Re = 2.85, 8.52 and 16.17) were simulated.

It took about 1/12 of the impeller revolution for the flow to become steady and converged. After that one impeller revolution was simulated (the first $1/12^{th}$ of the revolution was not considered in later evaluation).

The values ρ_{air} = 1.225 kg/m^3, ρ_{CMC} = 1000 kg/m^3, $\eta_{air} = 1.78*10^{-5}$ Pas and σ = 0.07 N/m for CMC and air density, air dynamical viscosity and surface tension respectively, were used for the simulation. A shear dependent viscosity (Eqn. 1) was used for the CMC.

COMPARISON BETWEEN EXPERIMENTAL RESULTS AND SIMULATION

Fig. 7 clearly depicts the periodic nature of the tangential velocity magnitude, which was measured by the LDA method (N = 60 rpm, measuring point r = 90 mm, z = 135 mm).

The tangential velocity is obviously related to the impeller rotating frequency. The period of the tangential velocity magnitude oscillations is 0.172 s, which is the approximately one period of a particular impeller blade passing through the vertical plane of the LDA measuring volume. Unexpected features regarding the tangential velocity time series are the measured short peaks of very high tangential velocity values. The tangential velocity of the impeller blade tip is v = 0.503 m/s at N = 60 rpm, whereas tangential velocity of the fluid at a point placed between the blade tip and the vessel wall (at r = 90 mm), exceeds this value (v = 0.525 m/s).

The fluid particle is obviously exposed to very high velocity gradients when the blade passes it. This phenomenon is interesting and its mechanism is still open for discussion. It can be seen from Fig. 6 that the duration of such a high velocity burst is very short, so the LDA system was not able to record each tangential velocity peak with the data rate present at the time of measurements (~ 5000 to 10000 particles per second). The increase of the tangential velocity at the blade transitions was confirmed with the results of numerical simulation (Figs. 8 to 10) as well, although the simulated velocity peaks are much smaller than those found in the experimental results.

The following results (Figs. 8 to 10) show the evolution of the tangential velocity with the peaks filtered out.

Fig. 8 shows the comparison between experimentally measured and numerically predicted tangential velocity distribution in points r = 90mm, z = 135 and 196 mm for rotational frequency N = 30 rpm.

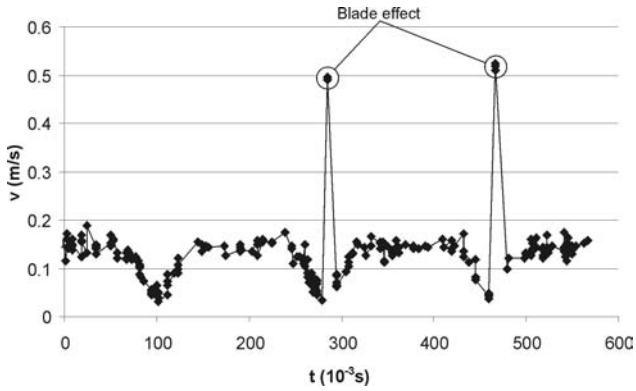

Figure 7: LDA measurements of tangential velocity for rotational frequency N = 60 rpm, measuring point r = 90, z = 135 mm.

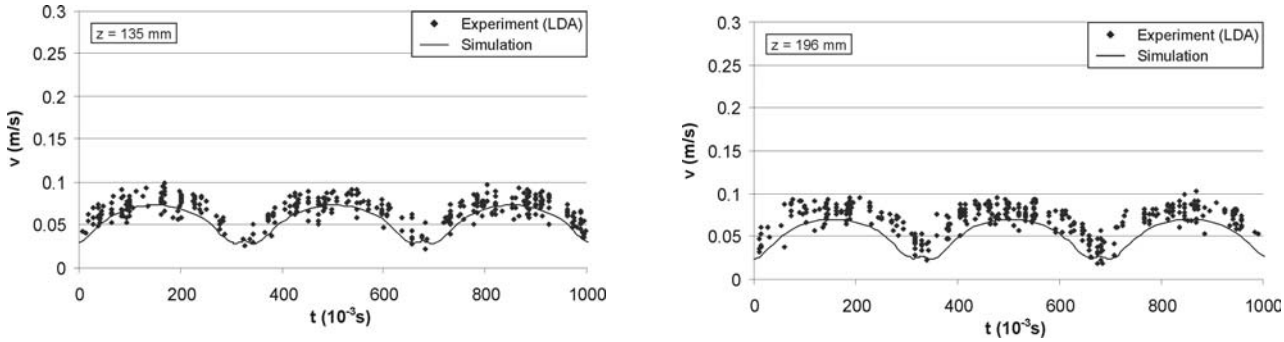

Figure 8: Experimentally determined and numerically predicted tangential velocity evolution in points r = 90mm, z = 135 (top) and 196 mm (bottom) for rotational frequency N = 30 rpm.

We can see that the numerically predicted tangential velocity follows the experimentally measured one. The period of oscillation is 0.32 s in the experiment and 0.33 s in the numerical simulation, which corresponds well to the period of blade transition. The maximal measured velocity value (excluding velocity peaks – Fig. 7 and point to point fluctuations) was 0.08 m/s. The measured velocity shows maximal fluctuations from point to point of about 0.03 m/s from the mean value. The reason for this is probably a combination of actual velocity fluctuations, measuring uncertainty and the fact that LDA method is usually not intended for unsteady measurements (despite the data rate was very high – 10 kHz). Results of simulation predict the tangential velocity to be about 10 % lower. The reason for the discrepancy could lie in the uncertainty of measuring volume position (even a small shift toward the vessel wall – to for example r = 90.5 mm results in about 10 % lower detected velocities, which correspond better to the simulation results). We can also see the before mentioned small peaks that are predicted at the blade transition. Both experiment and the numerical simulation show no significant difference in velocity evolution between planes z = 135 and z = 196 mm.

We can see the tangential velocity evolution in points r = 90mm, z = 135 and 196 mm for rotating frequency N = 60 rpm in Fig. 9.

As expected the tangential velocities are higher (maximal measured value is about 0.18 m/s (0.14 m/s in simulation) – excluding velocity peaks and point to point fluctuations). The period of oscillation is of course shorter - 0.172 s in the experiment and 0.166 s in numerical simulation. Small increases in the velocity at the blade transition are somewhat higher, but still for only about 10 %.

The evolution of the tangential velocities for the case of rotational frequency N = 90 rpm is shown in Fig. 10.

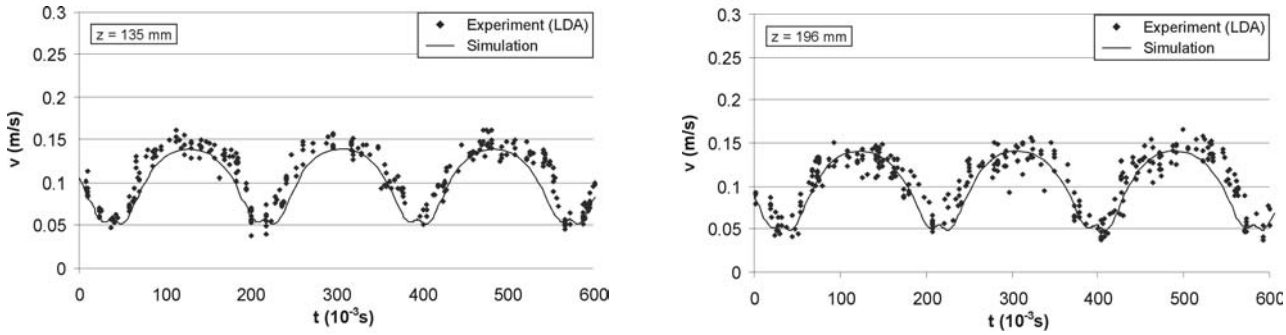

Figure 9: Experimentally determined and numerically predicted tangential velocity evolution in points r = 90mm, z = 135 (top) and 196 mm (bottom) for rotational frequency N = 60 rpm.

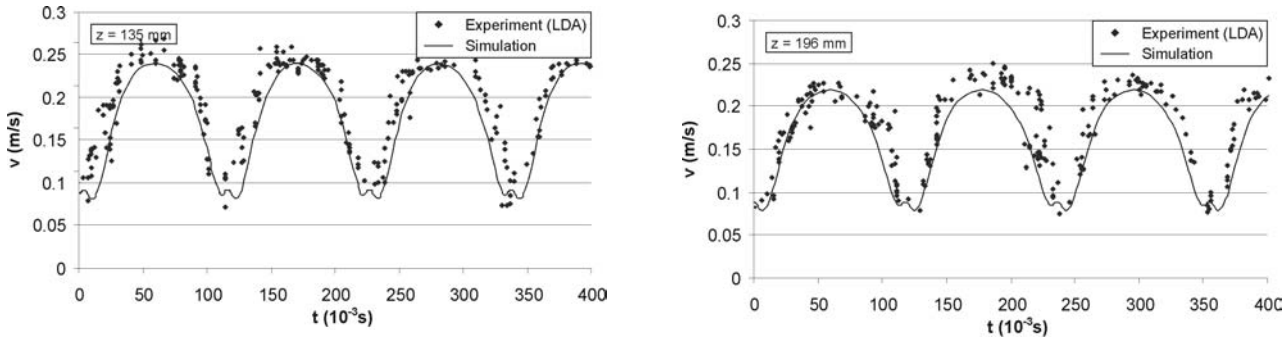

Figure 10: Experimentally determined and numerically predicted tangential velocity evolution in points r = 90mm, z = 135 (top) and 196 mm (bottom) for rotational frequency N = 90 rpm.

As a result of decrease of importance of accompanying effects like outer flow disturbances the point to point fluctuations decrease (Fig. 10). The period of oscillation is 0.117 s in the experiment and 0.111 s in numerical simulation. The numerically predicted tangential velocities are still about 10 % lower than the experimentally measured ones. The small velocity peaks that occur at blade transition are more evident – the velocity increases rapidly for approximately 17 %.

To investigate the possibility of numerical reproduction of the vortex above the impeller, pathlines leading from a point of tracer fluid injection (z = 150 mm) were plotted. Fig. 11 shows an image of the developed vortex (left), simulated vortex (middle) and the diagram where experimentally determined and numerically predicted vortex shapes are compared (right) for rotational frequencies 90 (above), 60 (middle) and 30 rpm (bottom). In the case of low rotational frequency (30 rpm) vortex did not evolve in the numerical simulation (probably due to the short simulation period). By plotting velocity vectors and indicating the probable flow path the expected evolution of the shape of the vortex can already be determined (middle bottom picture in Fig. 11).

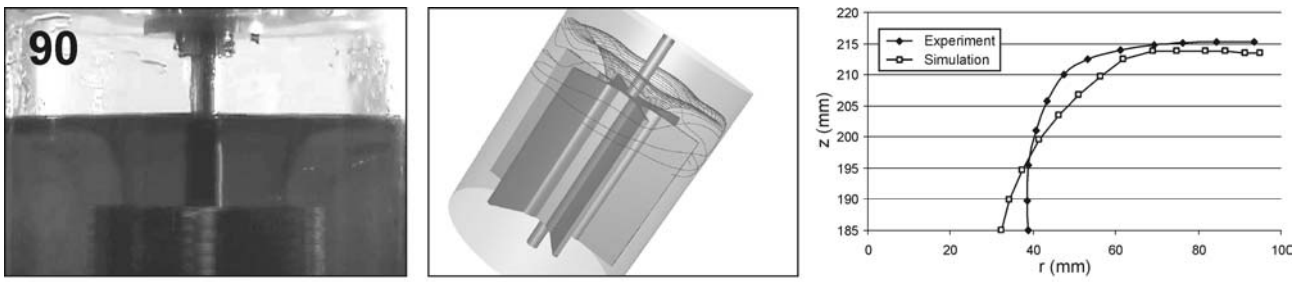

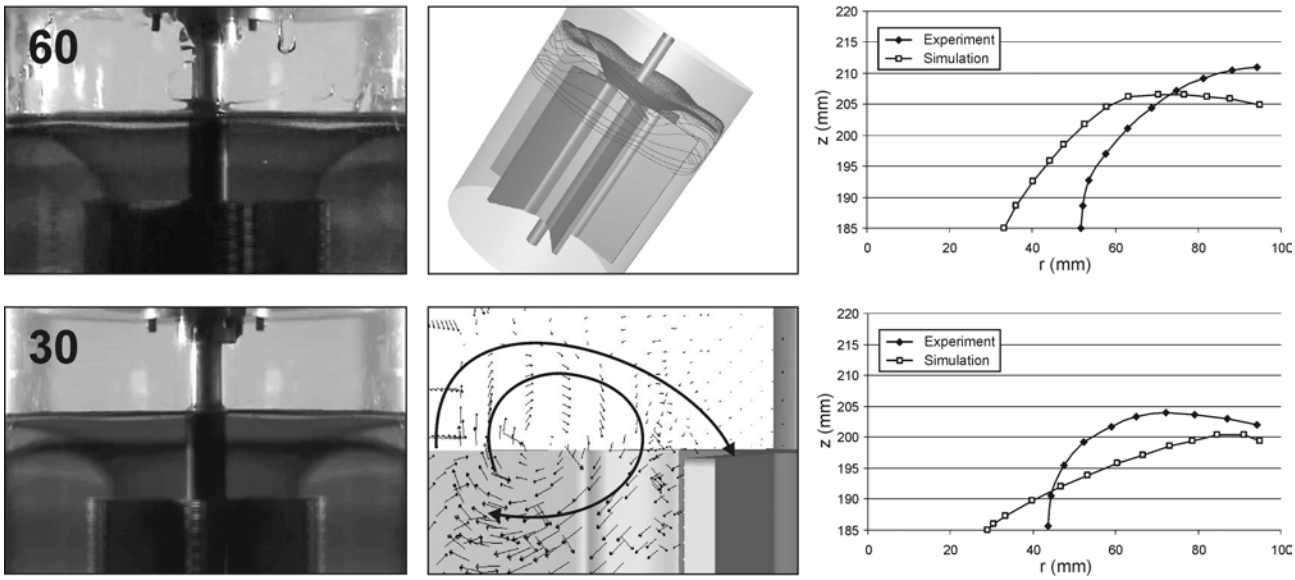

Figure 11: Experimentally observed and numerically predicted vortex above the impeller.

We can see that the radius of the vortex near the impeller becomes smaller when the rotational frequency is increased. The numerical simulation always predicts the vortex to have a flatter shape. Also the angle between the impeller and the vortex is smaller in the case of numerical prediction than in the case of experiment. The best correlation was achieved in the case of high rotational frequency of 90 rpm.

The reason for the vortex development was partially confirmed by the numerical simulation. Very small pressure difference exists on the vessel wall between free surface level and impeller level (Tab. 2). Due to the possible numerical error we cannot consider the absolute values of these pressure differences, but the trend is probably correct and it reveals the source of the small velocities and of the vortex formation.

It is also interesting that two vortices (one in another) exist in the case of rotational frequency 30 rpm. The reason for this is still unclear. The pressure differences are so small in this case (Tab. 2) that any small unavoidable disturbance (geometry flaws like scratches, unevenness of the surface and small discrepancies in axial symmetry of the impeller, small sudden shock or presence of small bubbles in the fluid) can cause the vortex to evolve differently. That is also the most probable reason for best correlation of the vortex shape at high rotational frequency (90 rpm) – in this case the unavoidable disturbances, that are not included in the numerical model, had less effect on the result – the experimental flow pattern is closer to the ideal one.

An isosurface with volume fraction $\alpha = 0.5$ was considered as a free surface found by the numerical simulation. It was estimated that the average difference between the positions of isosurfaces of $\alpha = 0.1$ and $\alpha = 0.9$ was less than 4%.

In general the predictions of the shapes of the surface can be seen as plausible (Fig. 12). The trends are correctly predicted but discrepancies exist. These are particularly evident near the shaft and the vessel wall, and are probably a result of discrepancies in surface tension, which results from mass diffusion effect, which is common in unsteady VOF simulations.

Fig. 13 shows experimentally measured and numerically predicted torque on the shaft of the impeller as a function of rotational frequency.

We can see that about 20 % discrepancy between the numerically predicted and experimentally measured torque on the impeller shaft exists. The numerically predicted torque is constantly smaller. The reason for the discrepancy is probably related to the tangential velocity prediction, where also smaller values were found. The small flaws in the geometry that were not included in the numerical model and uncertainty at the viscosity and rotational frequency measurements could also be influential.

Table 2: Comparison of tracer fluid z-velocity and pressure difference that causes the flow in point r = 95 (vessel wall), z = 196.

Rotational frequency (rpm)	Pressure difference (sim.) (Pa)	z-velocity (exp.) (mm/s)	z-velocity (sim.) (mm/s)
30	~ 0.011	3.7	4.5
60	~ 0.045	9.1	9.5
90	~ 0.093	14.0	13.5

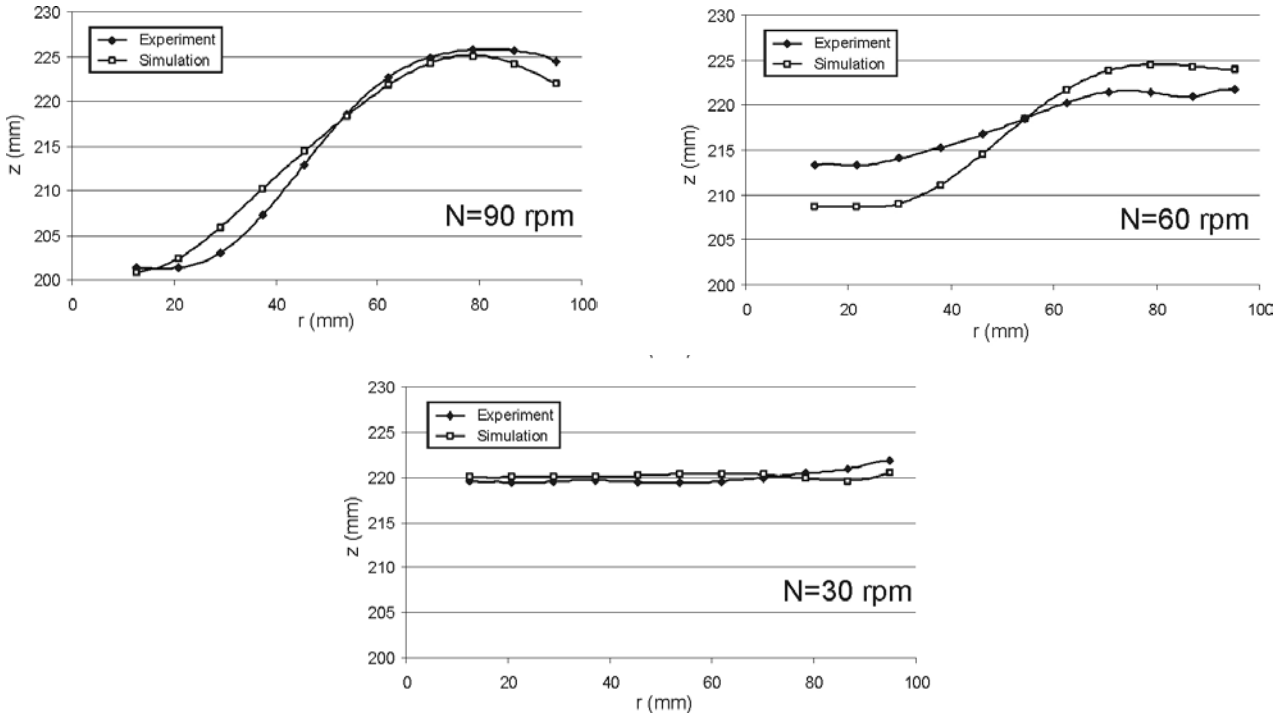

Figure 12: Experimentally determined and numerically predicted shape of the free surface.

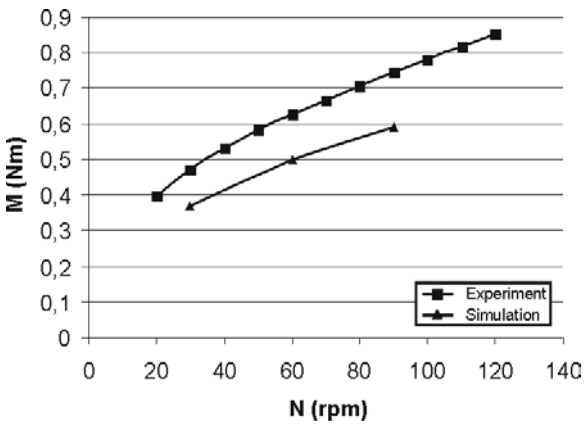

Figure 13: Experimentally measured and numerically predicted torque on the shaft of the impeller.

CONCLUSIONS

The characteristics of the flow induced by a six-bladed vane impeller were determined by LDA measurements. The periodic nature of the tangential velocity magnitude was clearly observed from time series of tangential velocities.

By injecting the tracer fluid the vortex above the impeller could be observed – its shape was determined by maximal gradient method.

Torque on the shaft of the impeller was measured and rheological properties (shear dependent viscosity) of the CMC solution were determined.

The purpose of the study was also to evaluate the capability of numerical simulation to predict different features of non-Newtonian fluid mixing process. The model included the mixing process, the shear dependent viscosity and the free surface problem. 3 simulations were performed.

The results of numerical simulation show good agreement to the experimental measurements. The numerically predicted tangential velocities are a bit smaller than experimentally measured ones. The simulations also predict a small increase of the velocity at the blade transition, which was sometimes observed at the experiment in a form of a high velocity peak. It was also possible (apart of rotational frequency N = 30 rpm) to predict the formation of vortex above the impeller. The numerically predicted vortex shape was flatter than the experimentally observed one.

The predictions of the shapes of the free surfaces were generally found to be correct. Only the case with N = 60 rpm showed greater discrepancies.

Probably due to the use of an ideal geometry, where small geometrical inaccuracies were not considered, the simulated torques on the shaft of the impeller are lower than the experimentally measured ones; the trend (torque vs. rotational frequency) is correctly predicted.

The results show that it is possible to relatively accurately predict many features of mixing non-Newtonian flow with a free surface. The gained knowledge of numerical simulation is applicable to optimisation of real mixing processes in industry where experimental measurements are difficult or impossible to perform.

NOMENCLATURE

A	gray level value	(-)
D	impeller diameter	(m)
D_T	vessel diameter	(m)
F	force	(N)
g	gravitational acceleration	(m/s^2)
h	impeller height	(m)
H	height of the fluid inside the vessel	(m)
i	coordinate in image	(-)
j	coordinate in image	(-)
K_s	impeller geometry constant	(-)
k	consistency index	(Pas)
N	rotational frequency	(s^{-1})
n	flow behaviour index	(-)
p	pressure	(Pa)
Re	Reynolds number	(-)
t	time	(s)
v	velocity	(m/s)
v_m	mixture velocity	(m/s)
Z	distance between the vessel bottom and blades	(m)
α_q	q-th phase volume fraction	(-)
σ	liquid surface tension	(N/m)
$\dot{\gamma}$	shear rate	(s^{-1})
η	dynamic viscosity	(Pas)
η_{ai}	air dynamic viscosity	(Pas)
η_m	mixture dynamic viscosity	(Pas)
ν	kinematic viscosity	(m^2/s)
ν_m	kinematic viscosity	(m^2/s)
ρ	density	(kg/m^3)
ρ_{air}	air density	(kg/m^3)
ρ_{CMC}	mixture density	(kg/m^3)
ρ_m	mixture density	(kg/m^3)

REFERENCES

Boyer F., Chupin L., Fabrie P., Numerical study of viscoelastic mixtures through a Cahn–Hilliard flow model, European Journal of Mechanics - B/Fluids, 23-5, 759-780 (2004).

Brito-de la Fuente E., Nava J. A., Lopez L. M., Medina L., Ascanio G., Tanguy P. A., Process Viscometry of complex fluids and suspensions with helical ribbon agitators, Can. J. Chem. Eng., 76, 689-695 (1998).

EKATO, Handbook of mixing technology, EKATO Ruehr - und Mischtechnik GmbH, Schopfheim (1991).

Fryer P. J., Pyle D. L., Rielly C.D., Chemical engineering of the food industry, Blackie Academic & Professional, London (1997).

Harnby N., Edwards M. F., Nienow A. W., Mixing in process industries, Butterworth-Heinemann Ltd, GB (1992).

Hirt C. W., Nichols B. D., Volume of Fluid (VOF) Method for the Dynamics of Free Boundaries, Journal of Computational Physics, 39, pp. 201-225 (1981).

Kelly W., Gigas B., Using CFD to predict the behavior of power law fluids near axial-flow impellers operating in the transitional flow regime, Chemical Engineering Science 58, 2141 – 2152 (2003).

Mavros P., Flow visualization in stirred vessels, A review of experimental techniques, Trans. IChemE, 79, Part A, 113-127 (2001).

Metzner A. B., Otto R. E., Agitation of non-newtonian fluids, AIChE J., 3, 3-10 (1957).

Shao S., Lo E. Y. M., Incompressible SPH method for simulating Newtonian and non-Newtonian flows with a free surface, Advances in Water Resources 26, 787–800 (2003).

Slemenik-Perše L., Laminar mixing and determination of the viscosity of complex fluids in a mixer, PhD work, Ljubljana (2004).

Slemenik Perše L., Žumer M., Mixing and viscosity determinations with helical ribbon impeller, CABEQ, 18 (4), 363-371 (2004).

Širok B., Bajcar T., Dular M., Reverse flow phenomenon in a rotating diffuser, J. flow vis. image process 9, no. 2/3, 193-210 (2002).